*remote sensing*

MDPI

*Article*

# Assessment of the Radiometric Calibration Consistency of Reflective Solar Bands between Terra and Aqua MODIS in Upcoming Collection-7 L1B

**Aisheng Wu [1,*], Xiaoxiong Xiong [2], Amit Angal [1], Qiaozhen Mu [1] and Sherry Li [1]**

[1] Science Systems and Applications, Inc., 10210 Greenbelt Rd., Lanham, MD 20706, USA; qiaozhen.mu@ssaihq.com (Q.M.); xuexia.chen@ssaihq.com (S.L.)
[2] Sciences and Exploration Directorate, NASA Goddard Space Flight Center, Greenbelt, MD 20771, USA; xiaoxiong.xiong-1@nasa.gov
* Correspondence: aisheng.wu@ssaihq.com

**Abstract:** Two MODIS sensors onboard the Terra and Aqua spacecraft have been successfully operating for over twenty-three and twenty-one years, respectively, providing the worldwide user community with high-quality imagery and radiometric Earth observations of the land, atmosphere, cryosphere, and oceans. This study provides an assessment of the radiometric calibration stability and consistency of Terra and Aqua MODIS RSB using the L1B from the upcoming Collection 7 release. Several independent vicarious approaches based on measurements from the Libya-4 desert, Dome C, DCC, and SNO are used to assess the calibration stability at the beginning of scan, nadir, and end of scan. Results indicate that both Terra and Aqua RSB are stable to within 1% over their mission periods. Comparison of the normalized reflectances with either a BRDF model or a common reference sensor provides a radiometric assessment of Terra and Aqua calibration consistency. Comparison results show the VIS/NIR bands are in good agreement around the nadir and at the beginning of the scan for all the approaches. For cases at the end of the scan, the agreement varies depending on the approach but is typically within ±2%. The differences observed in the SWIR bands are slightly larger than the VIS/NIR bands, which are likely due to their high sensitivity to atmospheric conditions and relatively larger electronic crosstalk impact on the Terra instrument.

**Keywords:** MODIS; reflective solar bands; reflectance; vicarious calibration

check for updates

**Citation:** Wu, A.; Xiong, X.; Angal, A.; Mu, Q.; Li, S. Assessment of the Radiometric Calibration Consistency of Reflective Solar Bands between Terra and Aqua MODIS in Upcoming Collection-7 L1B. *Remote Sens.* **2023**, *15*, 4730. https://doi.org/10.3390/rs15194730

Academic Editor: Prasad S. Thenkabail

Received: 25 July 2023
Revised: 5 September 2023
Accepted: 19 September 2023
Published: 27 September 2023

**Copyright:** © 2023 by the authors. Licensee MDPI, Basel, Switzerland. This article is an open access article distributed under the terms and conditions of the Creative Commons Attribution (CC BY) license (https://creativecommons.org/licenses/by/4.0/).

## 1. Introduction

The successful decades-long operation of the two moderate-resolution imaging spectroradiometer (MODIS) instruments on the Terra and Aqua spacecraft has played a vital role in Earth observations [1–4]. The quality and accuracy of the calibrated imagery produced by the two instruments throughout their operating lifetime require regular monitoring of their radiometric performance, which is achieved by the suite of onboard calibrators in both the reflective and thermal spectral regions [5,6]. Routine post-launch calibrations are performed for the MODIS reflective solar bands (RSB) using the solar diffuser (SD), moon, and vicarious targets, including the deserts, ocean, dome concordia (Dome C) in Antarctica, and deep convective clouds (DCC). Establishing a calibration consistency between the satellite measurements from the two instruments is essential in generating a multi-year data record for long-term monitoring of the Earth's land, oceans, atmosphere, and cryosphere.

Various techniques have been implemented to perform cross-calibration between satellite sensors, including the two MODIS instruments, in the reflective part of the spectrum [7–13]. One of the most popular techniques is the use of pseudo-invariant calibration sites (PICS), such as North African desert sites and the Dome C in Antarctica. More recently, the application of DCC has become widely used in long-term stability monitoring of satellite sensors and cross-calibration between sensors [14,15]. Other techniques include

the use of instrumented sites such as RadCalNet (the Radiometric Calibration Network portal, an initiative of the Working Group on Calibration and Validation of the Committee on Earth Observation Satellites) that provide an in situ as well as top-of-atmosphere (TOA) reflectance profile coincident with the satellite overpass time [16]. Another technique is the use of near nadir simultaneous overpasses (SNO) from a third sensor as a bridge to perform the cross-calibration between sensors that are in a different orbit and do not have widespread overlapping observations (such as Terra and Aqua) [9,10,17]. Early results based on SNO, the Libyan Desert, Dome C, and DCC show that the Terra and Aqua Collection-6 (C6) calibration has agreement within 1.2%, whereas in some cases, the C5 calibration exceeds 2% [14,18]. Bhatt et al. [15] presented a DCC-based calibration approach for an independent evaluation of the MODIS RSB response versus scan-angle (RVS) performance in C6.1. Their results show that the long-term calibration stability and RVS differences in C6.1 have been significantly improved for Aqua-MODIS RSB. Lyapustin el at. [19] used the multiangle implementation of the atmospheric correction (MAIAC) algorithm over deserts, and results showed that the C6 calibration approach removes major calibration trends in the C5 Level 1B (L1B) data. Their results revealed residual decadal trends on the order of several tenths of 1% in the C6 reflectance in the visible and near-infrared MODIS bands, as well as a systematic Terra-Aqua bias, which is up to 1.5% depending on the band. Levy et al. [20] compared MODIS C6 level 4 products of global aerosol optical depth (AOD) over both land and ocean between Terra and Aqua. Their results showed that the global monthly mean AOD from Terra is consistently higher than Aqua, and the relative offset has seasonal as well as long-term variability. After the Terra-to-Aqua cross-calibration methods [19] were applied, the overall AOD offset over land was significantly reduced but did not affect the overall offset over the ocean.

In this work, we present a brief overview of the MODIS RSB calibration algorithm, including some of the major improvements in the forthcoming release of the Collection 7 (C7) L1B algorithm. The C7 L1B algorithm incorporates major improvements in the estimation of the gain for the visible (VIS) and short-wave infrared (SWIR) bands of Terra MODIS that are expected to produce a radiometrically enhanced product. Details about the MODIS RSB calibration improvements can be found in the literature [21,22]. Various intercomparison techniques, such as simultaneous nadir overpasses with the Visible Infrared Imaging Radiometer Suite (VIIRS) instrument and using TOA measurements from Libya-4, Dome C, and DCC, are discussed in detail, along with the results from each method. Finally, a comparison of the results from multiple techniques is discussed, along with the uncertainties associated with each approach. An important outcome of this work is that it provides a detailed assessment of the radiometric calibration differences between the two MODIS instruments using the L1B products that are consistently processed using the C7 algorithm. Results of this study indicate that both Terra and Aqua RSB are stable to within 1% over their mission periods. Comparison results show the two sensors are in good agreement at the beginning of the scan (BOS), around the nadir (NAD), and near the end of the scan (EOS) for all the approaches, indicating an excellent on-orbit RVS characterization.

## 2. MODIS RSB Calibration

### *2.1. MODIS RSB Calibration Algorithm*

The calibration of MODIS RSB is performed by measuring the reflected sunlight from an onboard SD [5,6]. The bidirectional reflectance distribution function (BRDF) of the SD was characterized prelaunch. The degradation of the SD is monitored by the Solar Diffuser Stability Monitor (SDSM). The reflectance factor obtained from the Earth view (EV) port can be expressed as

$$\rho_{\mathrm{EV}} cos(\theta_{\mathrm{EV}}) = m_1 d_{\mathrm{ES}}^2 dn_{\mathrm{EV}} (1 + k_{\mathrm{Inst}} \Delta T_{\mathrm{Inst}}) / \mathrm{RVS} \quad (1)$$

where $\theta_{EV}$ is the solar zenith angle at the Earth View (EV), $m_1$ is the reflectance scaling factor determined from the SD calibration, $dn_{\mathrm{EV}}$ is the Earth view digital number corrected for instrument background, $d_{ES}$ is the Earth–Sun distance, $k_{\mathrm{Inst}} \Delta T_{\mathrm{Inst}}$ is the instrument

temperature variation correction, and RVS is the response versus scan angle normalized to the SD angle of incidence (AOI) relative to the scan mirror at an AOI of 50.25°. The baseline RVS was obtained from the prelaunch characterization, which is dependent on the band, detector, and mirror side. On-orbit temporal changes in RVS are measured at other AOIs besides the SD AOI. For most RSB bands, temporal changes in RVS are characterized using the lunar measurements obtained at the AOI of 11.25°. Since only two separate AOI angles at the SD and lunar views are used, a linearly dependent change in RVS is applied. For the remaining RSB, which are mainly at short wavelengths, the linear approach is insufficient to accurately characterize the RVS changes with scan angle after several years in operation, and therefore, supplemental responses at various AOI angles from pseudo-invariant desert sites are used [23,24]. At the SD AOI, an additional adjustment in gain is also applied based on the desert response data. This calibration approach was implemented in the generation of the C6 and C6.1 L1B products for both Terra and Aqua.

### *2.2. C7 Calibration Improvement over C6*

In C7, there are several major improvements in the calibration algorithm for Terra MODIS RSB [21,22]. Since Terra MODIS shows a significant increase in polarization sensitivity, particularly near the end of the scan, data from the desert sites are affected by increased fluctuations in the trends used to derive the RVS. Significant changes to the polarization sensitivity have been observed for Terra bands 3, 8, 9, and 10 [25,26]. To mitigate the impact of polarization on temporal trends of response for the desert sites, the desert responses are corrected using an algorithm developed by the NASA Ocean Biology Processing Group (OBPG) before their use in the RVS characterization [25]. The OBPG polarization correction was used initially to mitigate the impacts on ocean color products. In recent years, it has also been adopted by other science disciplines using Terra MODIS products. Adding the polarization correction has led to a significant reduction in the temporal fluctuation and an improvement in gain estimation for these bands at large AOIs.

In C6/6.1, the Terra MODIS visible and near-infrared (VIS and NIR) bands that rely on the use of supplemental responses from the desert sites to characterize the on-orbit RVS changes include bands 1–4 and 8–10. For C7, VIS bands 11 and 12 are added with results obtained from ocean observations, and a ratio approach is used to derive the on-orbit RVS with spectrally matching band 4 as a reference [21]. Results have shown that this approach improves the long-term reflectance drifts seen in C6/C6.1 calibration for the two bands. For Terra MODIS SWIR bands, there are two major improvements in C7. First, an enhanced crosstalk correction for the SWIR bands is applied over the entire mission by replacing band 28 as a sending band with band 25. This is due to an increased electronic crosstalk in band 28, and results showed that the enhanced algorithm has demonstrated a marked improvement in image quality and radiometric stability. Secondly, the SWIR bands rely on RVS determined from prelaunch in C6/6.1. In C7, a time-dependent change in RVS is applied using observations from the DCC to correct for the long-term drifts [22,27]. The DCC data are used to generate an on-orbit RVS for bands 5 and 26 and to correct inaccuracies of the SD calibration for all four SWIR bands 5–7 and 26. In the case of Aqua RSB, improvements mainly include the RVS fitting techniques. Since a polynomial fitting is used for RSB in their LUT generation on a routine basis, an entire mission reprocess with a consistent fitting mechanism reduces some of the uncertainties caused by the fitting predictions.

The data used in this study are based on the Level-1B product generated internally by the MODIS Characterization Support Team (MCST) using the C7 lookup tables (LUT). The C7 LUT has been internally tested and validated and has been delivered to NASA's MODIS Adaptive Processing System (MODAPS), where they are currently undergoing further science tests.

## 3. Methodology for Terra and Aqua Intercomparison

### *3.1. Libya-4 Desert*

Reflectances collected over the widely used Libya-4 desert site (28.5°N, 23.4°E) (Figure 1) [13,14,28,29] are used because of their high radiometric stability and spatial, spectral, and temporal uniformity. Three sets of overpasses at BOS, NAD, and EOS over the desert site are chosen for Terra and Aqua, respectively. Each set of overpasses contains data from repeatable orbits every 16 days that have the same view zenith angles for each instrument. This provides trends of reflectance with nearly identical view zenith angles and makes the correction of the bidirectional reflectance effect more efficient. Data are extracted from a 20 km × 20 km area surrounding the site at the pixel level and averaged for each band and mirror side. A pre-defined criterion (standard deviation from the mean <2%) is applied to examine the uniformity of the extracted pixels over the defined 20 km × 20 km area. Any overpasses over the site with standard deviations larger than the criteria are excluded. A site-dependent semi-empirical bi-directional reflectance function (BRDF) model is used based on two kernel-driven formulations provided by Roujean et al. [30].

$$R^i(\theta_{EV}, \varphi_{EV}, \psi_{EV}) = K_0^i + K_1^i f_1 + K_2^i f_2 \quad (2)$$

where $R$ is the modeled reflectance, $\varphi$ and $\delta$ are the viewing zenith and relative azimuth angles at the EV, respectively, $i$ is the index for the band, $f_1$ and $f_2$ are a series of kernel functions. For the Libya-4 desert site, $f_1$ and $f_2$ are based on Roujean's formulations. For the Dome C site, since the reflectance factors follow a simple linear r relationship with the solar zenith angle, a relatively simple formulation with only up to term $f_1$ is used. Coefficients $K_0$, $K_1$, and $K_2$ are surface type-specific coefficients determined empirically, which are derived from the multilinear regression using cumulative Aqua MODIS data over the initial five-year period in the mission. The BRDF-corrected reflectances are used to track the stability and perform the comparison of Terra/Aqua MODIS. Our early studies show that by restricting view zenith angles to a specific narrow range, the BRDF correction can reduce the impact of temporal variation to around 1% in the visible and infrared regions [14,18]. In the case of the SWIR bands, however, there are a few exceptions with a slightly large temporal variation (>1%) for some SWIR bands that have either a low signal level or higher sensitivity to atmospheric conditions.

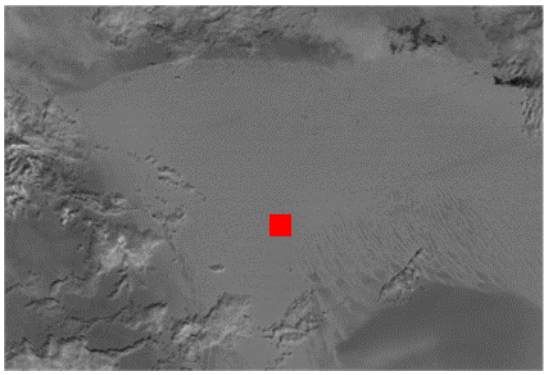


**Figure 1.** Image of region surrounding the Libya-4 site (highlighted red area of 20 km × 20 km) obtained from Terra MODIS band 1 at GMT 9:05 on 27 January 2022.

### *3.2. Dome C*

Another similar approach is based on reflectances collected over the Dome C site (75.1°S, 123.4°E) (Figure 2) located on the Antarctic Plateau. Dome C is one of the most homogeneous surfaces covered by snow and ice sheets [31,32]. Since MODIS is in a polar orbit, this approach has the advantage of more frequent overpasses over the polar region (during the Antarctic summer) than the Libya-4 desert site. There is about one near-nadir overpass per day available during the Antarctic summer. Like the desert approach, three

sets of overpasses at BOS (scan angle of −43.8°), NAD (scan angle of ~0°), and at EOS (scan angle of 46.4°) over the Dome C site are chosen for both Terra and Aqua. An average of reflectance collected over a 20 km × 20 km area (at nadir spatial resolution) centered at the Dome C site is calculated. Pre-determined spatial standard deviation (2% for most bands) in reflectance for the pixel window is used to remove overpasses that are suspected to be affected by clouds. For unsaturated bands, a further constraint of solar zenith angle < 80° is applied to reduce data fluctuation at high solar angles. Early studies [10,33] showed that a simple BRDF model expressed as a linear relationship with solar zenith angle works reasonably well, as shown in Figure 3.

$$R^i(\theta_{\mathrm{EV}}, \varphi_{\mathrm{EV}}, \psi_{EV}) = C_0^i(\theta_{\mathrm{EV}}, \varphi_{\mathrm{EV}}, \psi_{\mathrm{EV}}) + C_1^i(\theta_{\mathrm{EV}}, \varphi_{\mathrm{EV}}, \psi_{\mathrm{EV}})cos(\theta_{\mathrm{EV}}) \quad (3)$$



**Figure 2.** Image of region surrounding the Dome C site (highlighted red area of 20 km × 20 km) obtained from Terra MODIS band 1 at GMT 00:10 on 30 January 2022.

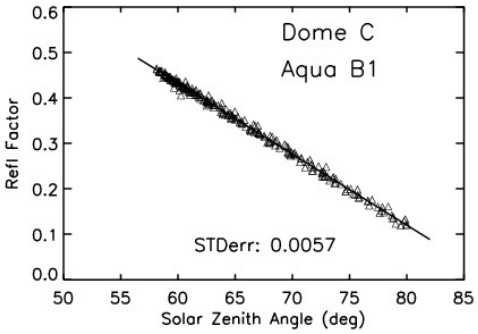



**Figure 3.** Relationship between reflectance factor and solar zenith angle for Aqua MODIS band 1 over the Dome C site. Each point in triangle represents one overpass, and data are collected from overpasses after 2018. Also shown are a linear regression line and the standard error.

The BRDF model's coefficients $C_0$ and $C_1$ are derived from the linear fit using cumulative Aqua MODIS data over the initial five-year period of the mission. The BRDF correction reduces the angular-dependent fluctuations by around 2% for the short visible bands and 2–3% for the remaining bands with longer wavelengths. In the case of the SWIR bands, results from the Dome C site are significantly noisier due to either a low signal level or high sensitivity to atmospheric conditions and are not included in this study.

### *3.3. DCC*

DCC are cold, bright targets consisting of high-reaching tropical cumulonimbus clouds in the tropopause. They are mainly over the tropics and can be considered to be near-Lambertian reflectors. DCC display consistent reflectance in the VIS/NIR spectrum with minimal impacts from water vapor and aerosols when viewed by sensors from space. Doelling et al. [34,35] developed a DCC technique that relies on a large-ensemble statistical approach, assuming the distribution of reflectance in the VIS/NIR spectrum remains constant in time. This approach was successful in the assessment of sensor calibration stability

and further extended to sensor intercomparison [10,35–38]. The potential DCC pixels are identified using the 11 μm (MODIS band 31) brightness temperature (BT) threshold of 205 K as a prerequisite in the tropical domain between 30°N and 30°S. All the DCC samples in this study are collected in the domain (30°S–30°N and 95°E–175°E) with a constraint of solar zenith angles less than 40°. The standard deviations of BT at 11 μm and visible reflectance at 0.65 μm (MODIS band 1) are computed over all 3 × 3 pixel blocks surrounding each potential DCC pixel. Then, a further constraint of the potential DCC pixel is applied to exclude any pixel if the BT standard deviation is larger than the threshold of 1.0 K or the reflectance standard deviation is larger than 3%.

The DCC approach tracks the time series of the monthly reflectances obtained from the non-Gaussian and asymmetric probability density functions (PDFs). Normally, the PDF mode (peak) or mean of the reflectances is used as a representative value for long-term stability monitoring and sensor intercomparison (Figure 4). It has been recognized that the mode reflectance corresponding to the PDF peak is superior for most VIS/NIR bands when there are more than one million DCC pixels in each monthly PDF. As a result, the mode values are used for pixels from near-nadir DCC measurements. For pixels from off-nadir measurements, however, the mean values are used to generate more stable trends because the number of available pixels is significantly less due to their smaller scan angle ranges than those near the nadir whose frame range is at least five times more than those at off-nadir scan angles. There are 13 different off-nadir scan angles (or frames) across the entire scan angle range, which are centered at frames 50, 150, 250, 350, 450, 550, 650, 750, 850, 950, 1050, 1150 and 1277. For each off-nadir angle, a frame range is restricted to 100, corresponding to a scan angle range of 8.1°. Our previous studies [10,36,37] have shown that the DCC-specific BRDF model given by Hu et al. [39] is effective in reducing the bidirectional reflectance effects due to the seasonal variability in the VIS and NIR bands and less effective for the SWIR bands. Thus, no BRDF correction is applied for the SWIR bands. Because of saturation, only the non-saturated Terra MODIS reflective solar bands 1, 3–7, 18, and 26 are used over DCC. In the case of Aqua, bands 1, 3–7, 17–19, and 26 are used.

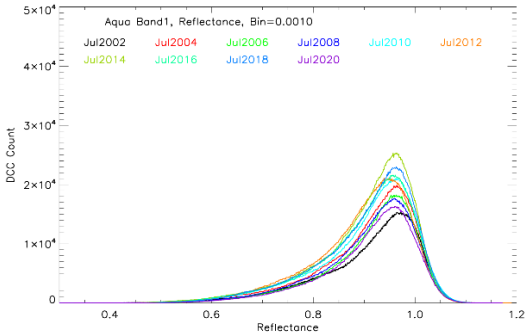
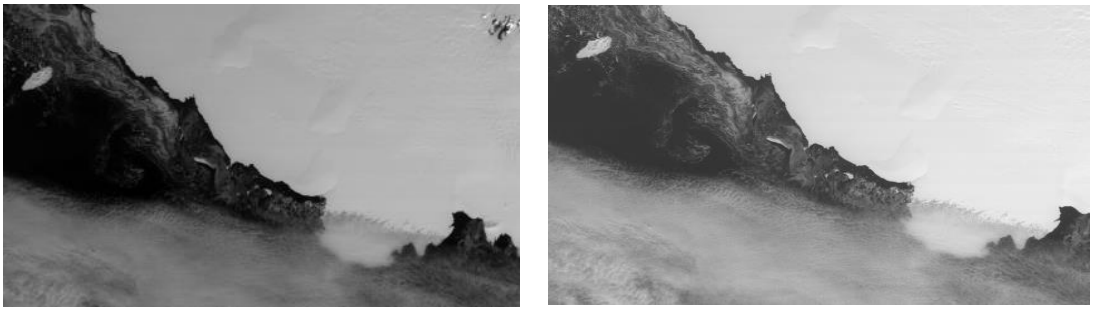



**Figure 4.** Monthly DCC PDF in reflectance from the near nadir view for Aqua MODIS band 1. The month of July every two years is selected.

### *3.4. SNO*

The last approach is based on SNO, which provides a direct pixel-level comparison between two crossover sensors [9,17,26]. Since there is no crossover between Terra and Aqua satellites, a third sensor is used as a transfer radiometer since it has a crossover with Terra and Aqua at different times. Our transfer radiometer relies on the Visible Infrared Imaging Radiometer Suite (VIIRS) that is being flown on the Suomi National Polar-orbiting Partnership (SNPP) spacecraft, launched in October 2011. There is an abundance of VIIRS and MODIS SNO, with nearly one SNO event every three or four days. The locations of Terra and SNPP SNOs are in the high-latitude region, while the SNO locations of Aqua and SNPP occur from the polar to relatively lower latitude areas. Figure 5 illustrates two crossover images from Aqua MODIS and SNPP VIIRS. The SNO data sets collected in this

study are restricted to the MODIS and VIIRS crossovers with a time difference of less than 180 s. An averaged ratio of reflectance between VIIRS and MODIS is determined once the number of matched pixels obtained from the geolocation of each SNO pair is statistically sufficient. Similar to the desert and Dome C sites, a pre-defined standard deviation limit is applied for data quality control to exclude the SNO events with larger standard deviations (>2.5%). Since there is no restriction of SNO on location and surface type, the results of this approach contain data from a wide variety of scene types. Figure 6 shows a typical example of pixel-to-pixel comparison of reflectance at 0.41 μm between SNPP VIIRS band M1 and Aqua MODIS band 8 based on an SNO event from 3 March 2022. The reason that the matched VIIRS and MODIS data are extracted at the pixel level is to exclude saturated pixels in the MODIS high-gain bands, which are mainly used in the retrieval of ocean color products. This allows the use of more MODIS bands in the SNO approach. Further discussion of the distinct advantages and disadvantages of each of the four approaches can be found in our previous studies [13,26].



(**a**) (**b**)

**Figure 5.** Images of one matched SNO pair of Aqua MODIS band 8 (**a**) and SNPP VIIRS band M1 (**b**). The Aqua image is obtained from an overpass at GMT 14:05 on 3 March 2022, and the SNPP image is at GMT 14:06 on the same date. To illustrate the overlapping of the two images, two small sub-sets of images extracted from a coast region in the Antarctica ocean near longitude 20.0°E are selected.

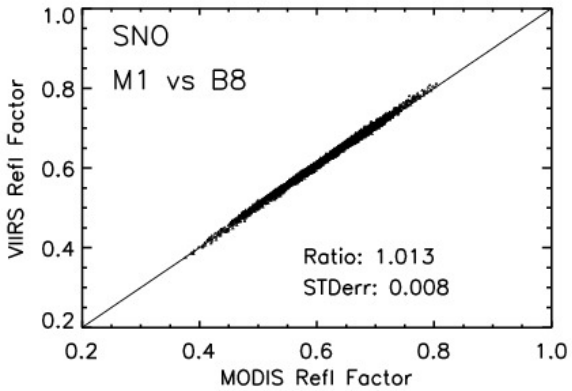



**Figure 6.** Example of pixel-to-pixel comparison of reflectance between Aqua MODIS band 8 and SNPP VIIRS band M1 obtained from one SNO event at 14:05 GMT on 3 March 2022. Numbers shown in the figure are values of the averaged VIIRS to MODIS reflectance ratio and standard error.

The impact on the various intercomparison results due to existing differences in the relative spectral response between Terra and Aqua RSB is negligible. Results based on the spectral band adjustment factor (SBAF) tool provided by NASA-LaRC (see link at https://cloudsgate2.larc.nasa.gov/cgibin/site/showdoc?mnemonic=SBAF, accessed on 15 August 2022) indicate that differences in SBAF derived from Terra and Aqua are within 0.1%. Therefore, no correction is applied for the spectral differences between Terra and Aqua RSB.

Comparison between Terra and Aqua is determined using the BRDF corrected reflectances for the Libya-4 and Dome C sites and DCC to remove the impact of differences in viewing and solar illumination angles on the comparison. For SNO, ratios of the MODIS reflectances to the reference sensor are used. A difference in reflectance between Terra and Aqua is determined:

$$D_{\mathrm{EV}}^{i,j} = \frac{\rho^{T}\left(\theta^{i}{}_{\mathrm{EV}}, \varphi^{i}{}_{\mathrm{EV}}, \psi^{i}{}_{\mathrm{EV}}\right)}{R\left(\theta^{i}{}_{\mathrm{EV}}, \varphi^{i}{}_{\mathrm{EV}}, \psi^{i}{}_{\mathrm{EV}}\right)} - \frac{\rho^{A}\left(\theta^{j}{}_{\mathrm{EV}}, \varphi^{j}{}_{\mathrm{EV}}, \psi^{j}{}_{\mathrm{EV}}\right)}{R\left(\theta^{j}{}_{\mathrm{EV}}, \varphi^{j}{}_{\mathrm{EV}}, \psi^{j}{}_{\mathrm{EV}}\right)} \quad (4)$$

where $R$ is the BRDF for the Libya-4, Dome C, and DCC approaches and the reflectance of the reference sensor for the SNO approach, and superscripts "$T$" and "$A$" represent Terra and Aqua, respectively.

## 4. Results

### *4.1. VIS and NIR Bands*

Trends of near-nadir reflectance for the shortest wavelength band 8 (0.41 μm) obtained from the vicarious approaches are shown in Figure 7. For the desert and Dome C sites, a site-dependent BRDF model derived using Aqua MODIS reflectance data is applied to both Terra and Aqua reflectances. Therefore, the Aqua reflectance trends are normalized to 1 at the beginning of the mission. To better illustrate the overall trend, each data point is an average over a year. For the DCC approach, since the impact of BRDF is much less than that for the desert and Dome C sites, no BRDF correction is applied to the data before the calculation of the yearly average. For the SNO result, since it is based on a ratio approach with SNPP VIIRS serving as a transfer reference, the impact of BRDF on the reflectances is largely removed, and there is no additional BRDF correction applied to the data. Each SNO data point is the average of a single crossover event and not a yearly average because SNPP VIIRS data are only available after January 2012. For band 8 (high gain ocean color band), no data are available from the DCC approach due to saturation. Trending results from 20-plus years of observations indicate excellent stability for both Terra and Aqua MODIS, with a total reflectance drift of less than 1% over the mission. Table 1A provides a summary of the stability assessment at the nadir view for both Aqua and Terra for C7. Except for a few bands for Terra over the Dome C site, all bands maintain excellent stability. In comparison with C6.1, the C7 stability is slightly improved due to the use of a consistent set of LUT over the mission, particularly for Terra VIS and NIR bands. For Terra band 8, on-orbit changes in polarization sensitivity are only significant near the end of the scan and do not impact these near-nadir results. Trending results indicate that the desert site and DCC are superior to the Dome C site in tracking satellite sensor calibration performance due to their relatively low uncertainties. Comparison of the normalized reflectances by either BRDF or a common reference sensor provides an assessment of the relative consistency of radiometric calibration between Terra and Aqua. For the SNO approach, there are a few residual effects that are considered minor, including differences in pixel footprint size, small but systematic angular mismatch between MODIS and the reference sensor, and the remaining atmospheric effect. Comparison indicates Terra and Aqua band 8 agree well within 2%, with Terra reflectances being higher than Aqua for the three approaches. Results for a NIR band (band 2 at 0.865 μm) are shown in Figure 8. There are no results for band 2 from DCC due to partial saturation early in the mission. For the NIR band, there is a similar agreement for the relative radiometric consistency as shown for the VIS band.

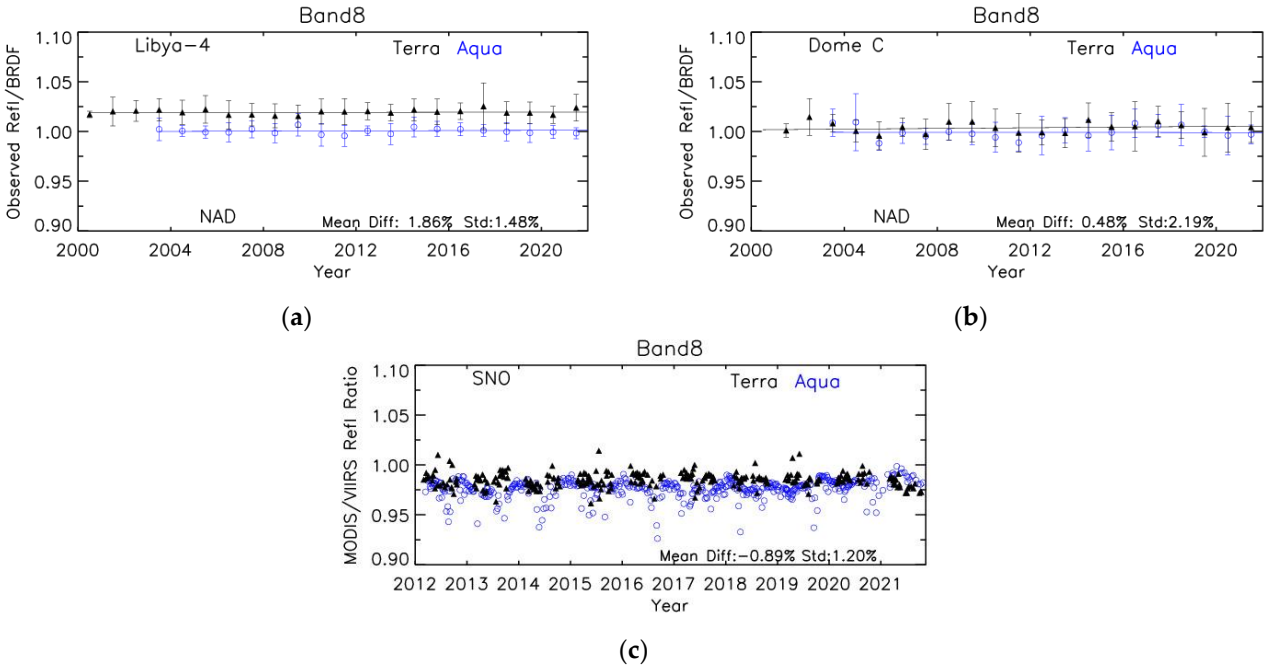



**Figure 7.** Normalized reflectance trends for Terra (solid triangle) and Aqua (open circle) MODIS band 8 (0.41 μm) obtained from Libya-4 (**a**), Dome C (**b**), and SNO with SNPP VIIRS (**c**). Error bars are the standard deviation.

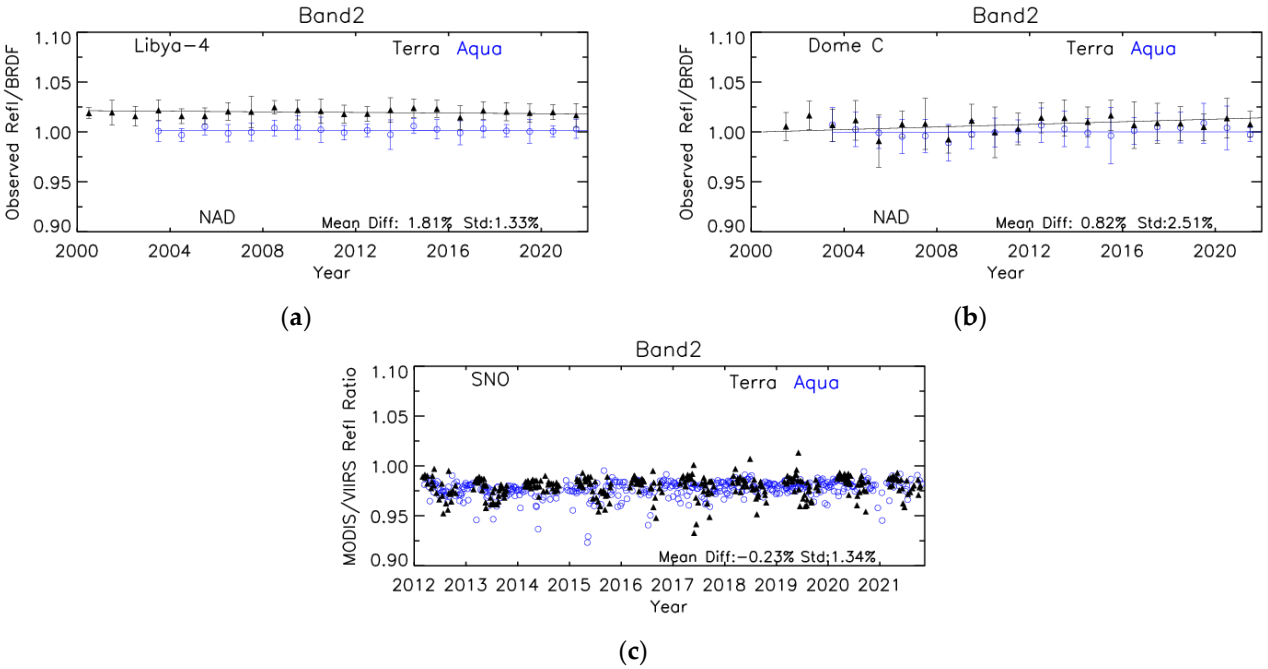



**Figure 8.** Normalized reflectance trends for Terra (solid triangle) and Aqua (open circle) MODIS band 2 (0.865 μm) obtained from Libya-4 (**a**), Dome C (**b**), and SNO with SNPP VIIRS (**c**).

### *4.2. SWIR Bands*

A major improvement for SWIR bands occurred on Terra due to a replacement of a prelaunch-based RVS with an on-orbit RVS and better characterization of the electronic crosstalk correction. As a result, there is a significant improvement over C6.1 (Table 1A,B) in the stability for Terra bands 5, 7, and 26. Results from a SWIR band (band 5 at 1.24 μm) for C7 are shown in Figure 9, which include the trends from the desert, SNO, and DCC approaches. Results from the Dome C approach are not included due to its exceptionally

high uncertainty. For SWIR bands, the DCC approach has a few distinct advantages over other approaches, including its high signal levels, low solar zenith angles, and less impact by the atmosphere. MODIS SWIR bands are known to be affected by an out-of-band thermal leak from the 5.3 μm wavelength region and electronic crosstalk with sending signal from the mid-wave infrared bands co-located in the same focal plane. The impact of the Terra SWIR crosstalk is known to be significantly larger than Aqua. As a result, a linear algorithm of crosstalk correction was designed early in the mission and implemented in the MODIS L1B calibration. For the Terra SWIR crosstalk correction in C7, a switch of sending band from band 28 (7.33 μm) to 25 (4.52 μm) further enhances the algorithm performance [40]. Due to the impact of the thermal leak and electronic crosstalk, it is expected that the SWIR radiometric differences between Terra and Aqua are larger than those for the VIS and NIR bands. Figure 9 shows an agreement of within 2% between Terra and Aqua for band 5. However, differences for the other three SWIR bands are up to 3%.

**Table 1.** (**A**) Terra and Aqua MODIS RSB stability for C7. Results are based on trending results at nadir and provided in percentage difference (%) over the mission for Libya-4, DCC, and Dome C. For each of the three approaches, results from the first row are for Aqua, and those from the second row are for Terra. Note results from DCC for bands 2, 8, and 9 and Dome C for band 9 are not available due to saturation. Results from bands 5–7 and 26 (SWIR bands) for Dome C are excluded due to their high uncertainties. (**B**) Terra and Aqua MODIS RSB stability is the same as Table 1A but for C6.1.

**(A)**

| Band | | 1 | 2 | 3 | 4 | 8 | 9 | 5 | 6 | 7 | 26 |
|---|---|---|---|---|---|---|---|---|---|---|---|
| **Libya-4** | **Aqua** | **−0.13** ±0.89 | **0.03** ±0.91 | **−0.18** ±0.94 | **−0.33** ±0.93 | **0.13** ±0.87 | **−0.13** ±0.89 | **−0.11** ±0.82 | **0.22** ±0.86 | **−0.51** ±1.80 | |
| | **Terra** | **−0.21** ±0.90 | **−0.28** ±0.95 | **−0.05** ±0.98 | **−0.40** ±0.91 | **0.02** ±1.18 | **−0.07** ±1.05 | **−0.86** ±0.95 | **−0.65** ±0.66 | **−0.36** ±1.88 | |
| **DCC** | **Aqua** | **−0.23** ±0.76 | | **0.82** ±0.75 | **0.42** ±0.78 | | | **0.02** ±0.57 | **0.80** ±1.62 | **0.38** ±2.36 | **0.17** ±1.59 |
| | **Terra** | **−0.75** ±0.57 | | **0.27** ±0.64 | **−0.37** ±0.69 | | | **−0.06** ±0.46 | **0.14** ±1.30 | **0.41** ±1.70 | **0.01** ±1.05 |
| **Dome C** | **Aqua** | **−0.22** ±1.77 | **0.03** ±1.73 | **−0.01** ±0.95 | **0.06** ±2.03 | **−0.03** ±1.45 | | | | | |
| | **Terra** | **1.22** ±1.84 | **1.24** ±1.82 | **1.19** ±1.22 | **1.01** ±2.05 | **0.33** ±1.64 | | | | | |

**(B)**

| Band | | 1 | 2 | 3 | 4 | 8 | 9 | 5 | 6 | 7 | 26 |
|---|---|---|---|---|---|---|---|---|---|---|---|
| **Libya-4** | **Aqua** | **0.07** ±0.88 | **0.25** ±0.91 | **−0.33** ±0.95 | **−0.26** ±0.94 | **−0.84** ±0.90 | **−0.44** ±0.92 | **−0.22** ±0.83 | **0.22** ±0.88 | **−0.56** ±1.81 | |
| | **Terra** | **−0.34** ±0.91 | **−0.67** ±0.96 | **0.76** ±0.99 | **−0.79** ±0.89 | **0.40** ±1.24 | **−0.48** ±1.11 | **1.78** ±0.95 | **0.17** ±0.66 | **2.90** ±1.90 | |
| **DCC** | **Aqua** | **−0.04** ±0.70 | | **0.59** ±0.72 | **0.43** ±0.74 | | | **−0.08** ±0.55 | **0.75** ±1.56 | **0.11** ±2.35 | **−0.08** ±1.52 |
| | **Terra** | **−0.75** ±0.60 | | **1.38** ±0.67 | **−0.16** ±0.64 | | | **2.27** ±0.50 | **0.78** ±1.25 | **2.82** ±1.68 | **2.41** ±1.07 |
| **Dome C** | **Aqua** | **−0.01** ±1.77 | **0.33** ±1.73 | **−0.13** ±0.95 | **0.13** ±2.03 | **−0.94** ±1.46 | | | | | |
| | **Terra** | **1.23** ±1.85 | **0.97** ±1.82 | **2.24** ±1.24 | **1.83** ±2.04 | **0.80** ±1.63 | | | | | |

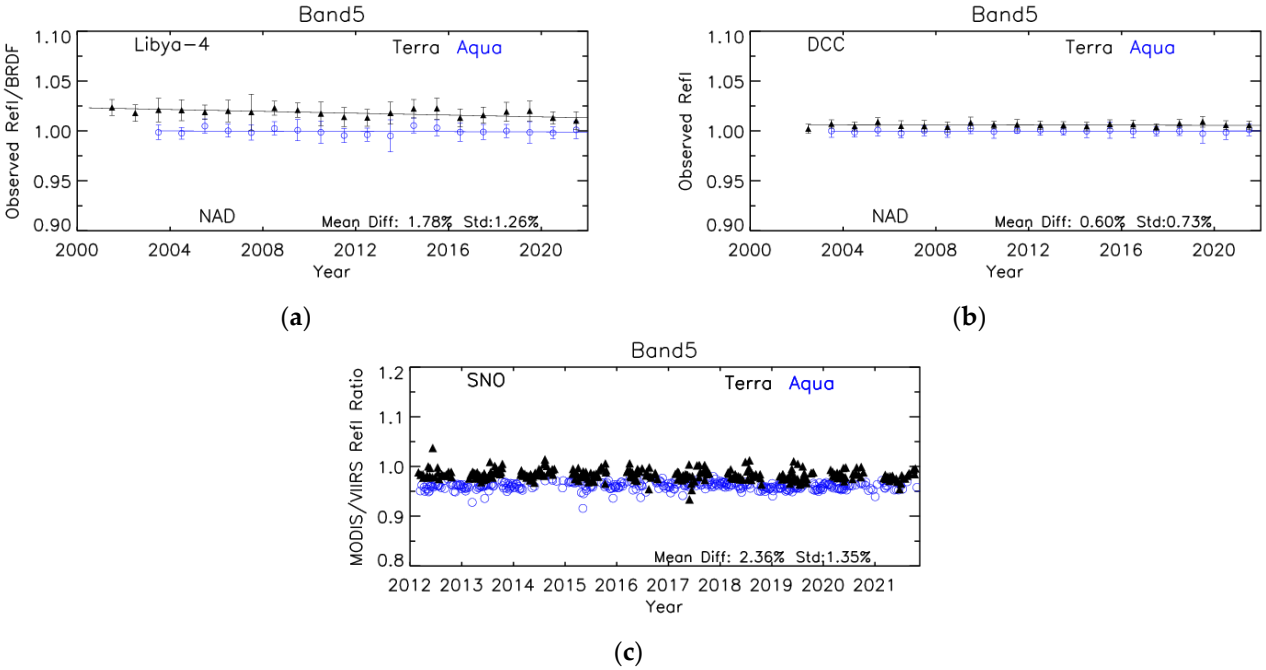



**Figure 9.** Normalized reflectance trends for Terra (solid triangle) and Aqua (open circle) MODIS band 5 (1.24 μm) obtained from Libya-4 (**a**), DCC (**b**), and SNO with SNPP VIIRS (**c**).

Current results indicate Terra and Aqua VIS/NIR bands have an agreement of within 2% at the nadir view for all the approaches in C7, as shown in Table 2A. In comparison with C6.1 (Table 2B), although there is a similar agreement between the two sensors, C7 is more consistent for the VIS/NIRS bands at this view angle range across different bands among the four approaches.

### *4.3. Beginning and End of Scan*

Results of intercomparison are further extended to the beginning and end of the scan to ensure a consistent radiometric calibration across the entire scan range. The purpose of examining results near the scan edges is that there is a large on-orbit correction for changes in the RVS. Changes are up to 20% in RVS (compared with more than 50% for gain correction) in the shortest wavelength bands. For the beginning of the scan, data are collected from a pixel window centered around a scan angle of −43.8° for the desert, Dome C, and DCC approaches, except for a scan angle of −41.5° used for Terra over the Libya-4 site. For the end of the scan, data are collected from a pixel window centered between scan angles of 46.1° and 48.7°, depending on the approach. There are no SNO results at either BOS or EOS due to difficulty in obtaining the matched pixel data for both Terra and Aqua with nearly the same off-nadir view angles. For the desert and Dome C approaches the site-dependent BRDF models are derived separately at BOS and EOS. Examination of the consistency of sensor and solar angles in BOS and EOS observations between Terra and Aqua indicates that the relative azimuth angles for the desert site do not overlap (one is from the forward and the other is from the backward direction), particularly for the EOS data. The impact of differences in the relative azimuth angle is considered negligible for near-nadir observations, but the effect is larger when increasing the off-nadir view angle if the surface is not Lambertian. This could add additional errors in the comparison results because the relative azimuth angles used in the derivation of the BRDF model do not cover the angular range for both Terra and Aqua. Figure 10 provides results of BOS and EOS for the shortest wavelength VIS band 8 (0.41 μm) obtained from the desert and Dome C sites. Results from the DCC are from unsaturated band 3 (0.44 μm). For the VIS bands, results generally show a consistent agreement between Terra and Aqua across the entire scan range. Band 3 shows a slightly larger difference (~3%) at BOS, and the bias is consistent

over the entire mission. Since the RVS is referenced to the prelaunch result, errors in the prelaunch RVS characterization would be carried forward in the on-orbit measurements. For band 8, larger uncertainties are observed at EOS than those at BOS. This is likely related to an increased polarization sensitivity towards the end of the scan based on the prelaunch tests for both Terra and Aqua. For Terra, it has been observed that there is a significant increase in on-orbit polarization sensitivity near EOS in the shortest visible wavelength range after 2008, which contributes to additional uncertainties at EOS. For Terra band 3, a noticeable increase in data fluctuation at EOS is observed, but its magnitude is much less than in band 8.

**Table 2.** (**A**) Terra and Aqua MODIS RSB comparison for C7. Results are provided in percentage difference (Terra—Aqua) (%). Numbers within the bracket are standard errors. (**B**) Terra and Aqua MODIS RSB comparison for C6.1. Results are provided in percentage difference (Terra—Aqua) (%). Numbers within the bracket are standard errors. "N/A" refers to not available.

| **(A)** | | | | | | | | | | |
|---|---|---|---|---|---|---|---|---|---|---|
| | **Desert** | | | **Dome C** | | | | **DCC** | | **SNO** |
| | **BOS** | **NAD** | **EOS** | **BOS** | **NAD** | **EOS** | **BOS** | **NAD** | **EOS** | **NAD** |
| **Band1** | **1.01** ±1.42 | **1.00** ±1.27 | **−2.46** ±1.64 | **0.23** ±3.95 | **0.18** ±2.56 | **−0.66** ±3.73 | **2.12** ±1.73 | **0.10** ±0.91 | **1.18** ±2.04 | **0.26** ±1.36 |
| **Band2** | **1.07** ±1.63 | **1.81** ±1.33 | **−0.97** ±1.60 | **0.33** ±3.59 | **0.82** ±2.52 | **0.34** ±4.02 | N/A | N/A | N/A | **0.26** ±1.39 |
| **Band3** | **1.55** ±1.23 | **2.22** ±1.37 | **−0.93** ±2.35 | **0.60** ±2.83 | **1.44** ±1.56 | **0.92** ±3.59 | **3.05** ±1.72 | **1.34** ±0.98 | **1.98** ±1.94 | **2.33** ±4.02 |
| **Band4** | **1.08** ±1.29 | **0.79** ±1.31 | **−3.84** ±1.94 | **−0.34** ±4.31 | **0.10** ±2.89 | **−1.43** ±3.98 | **1.74** ±1.68 | **0.10** ±0.99 | **0.35** ±1.97 | **−0.56** ±0.91 |
| **Band8** | **−0.10** ±1.38 | **1.86** ±1.48 | **−0.14** ±2.73 | **−0.74** ±2.70 | **0.49** ±2.21 | **0.61** ±5.23 | N/A | N/A | N/A | **0.90** ±1.21 |
| **Band9** | **0.24** ±1.25 | **1.04** ±1.39 | **−1.39** ±2.51 | **−0.59** ±3.14 | **−0.80** ±4.94 | **2.44** ±6.55 | N/A | N/A | N/A | **1.18** ±1.38 |
| **Band10** | N/A | N/A | N/A | N/A | N/A | N/A | N/A | N/A | N/A | **0.62** ±2.36 |
| **Band11** | N/A | N/A | N/A | N/A | N/A | N/A | N/A | N/A | N/A | **−1.75** ±4.21 |
| **Band12** | N/A | N/A | N/A | N/A | N/A | N/A | N/A | N/A | N/A | **0.09** ±2.86 |
| **Band5** | **1.18** ±1.38 | **1.79** ±1.26 | **−1.14** ±1.38 | N/A | N/A | N/A | **1.46** ±1.18 | **0.61** ±0.73 | **1.66** ±2.42 | **2.20** ±1.27 |
| **Band6** | **0.81** ±1.00 | **1.16** ±1.09 | **−0.53** ±1.07 | N/A | N/A | N/A | **−0.10** ±2.73 | **0.10** ±2.07 | **−0.61** ±5.62 | **0.66** ±4.51 |
| **Band7** | **−0.10** ±3.44 | **2.28** ±2.63 | **−0.11** ±3.18 | N/A | N/A | N/A | **−3.26** ±3.55 | **−3.12** ±2.88 | **−3.50** ±7.71 | N/A |
| **Band26** | N/A | N/A | N/A | N/A | N/A | N/A | **3.74** ±2.31 | **2.02** ±1.91 | **3.05** ±3.32 | N/A |

**Table 2.** *Cont.*

| | (B) | | | | | | | | | |
|---|---|---|---|---|---|---|---|---|---|---|
| . | Desert | | | Dome C | | | DCC | | | SNO |
| | **BOS** | **NAD** | **EOS** | **BOS** | **NAD** | **EOS** | **BOS** | **NAD** | **EOS** | **NAD** |
| **Band1** | **0.40** ±1.42 | **−0.07** ±1.27 | **−3.87** ±1.66 | **−0.41** ±3.92 | **−0.97** ±2.55 | **−2.01** ±3.71 | **1.37** ±1.71 | **−1.17** ±0.92 | **−0.27** ±2.04 | **−1.08** ±1.33 |
| **Band2** | **1.32** ±1.63 | **1.22** ±1.33 | **−1.29** ±1.60 | **0.56** ±3.56 | **0.08** ±2.51 | **0.05** ±4.00 | N/A | N/A | N/A | **−0.65** ±1.38 |
| **Band3** | **0.83** ±1.24 | **1.65** ±1.38 | **−2.26** ±2.46 | **−0.04** ±2.81 | **0.92** ±1.57 | **−0.16** ±3.53 | **2.33** ±1.69 | **0.76** ±0.99 | **2.41** ±2.01 | **1.33** ±3.16 |
| **Band4** | **1.04** ±1.30 | **0.54** ±1.30 | **−3.81** ±2.00 | **−0.35** ±4.28 | **−0.22** ±2.88 | **−1.45** ±3.97 | **1.70** ±1.67 | **−0.36** ±0.98 | **0.56** ±1.99 | **−0.83** ±0.78 |
| **Band8** | **−0.83** ±1.39 | **1.20** ±1.55 | **5.59** ±3.12 | **−1.49** ±2.66 | **−0.08** ±2.18 | **6.07** ±5.34 | N/A | N/A | N/A | **−0.14** ±1.72 |
| **Band9** | **−0.36** ±1.27 | **0.76** ±1.45 | **0.58** ±2.79 | **−1.20** ±3.10 | **−0.92** ±4.97 | **4.32** ±6.69 | N/A | N/A | N/A | **0.43** ±1.65 |
| **Band10** | N/A | N/A | N/A | N/A | N/A | N/A | N/A | N/A | N/A | **−0.26** ±2.25 |
| **Band11** | N/A | N/A | N/A | N/A | N/A | N/A | N/A | N/A | N/A | **−4.49** ±5.30 |
| **Band12** | N/A | N/A | N/A | N/A | N/A | N/A | N/A | N/A | N/A | **−1.51** ±4.36 |
| **Band5** | **2.53** ±1.39 | **2.80** ±1.28 | **−0.99** ±1.40 | N/A | N/A | N/A | **2.84** ±1.21 | **1.57** ±0.75 | **0.12** ±2.39 | **3.91** ±1.38 |
| **Band6** | **0.97** ±1.01 | **1.32** ±1.11 | **−0.37** ±1.09 | N/A | N/A | N/A | **1.92** ±2.74 | **2.52** ±2.00 | **−0.30** ±5.58 | **1.85** ±3.53 |
| **Band7** | **0.11** ±3.47 | **3.48** ±2.67 | **1.05** ±3.23 | N/A | N/A | N/A | **−2.17** ±3.57 | **−2.16** ±2.87 | **−2.25** ±7.65 | N/A |
| **Band26** | N/A | N/A | N/A | N/A | N/A | N/A | **4.71** ±2.35 | **2.98** ±1.88 | **3.85** ±3.33 | N/A |

Figure 11 shows the results of the comparison for SWIR band 5 at BOS and EOS over the Libya-4 desert and DCC. Results from the Dome C approach are not included due to their large uncertainties. As discussed previously, an electronic crosstalk correction with sending signal from the mid-wave infrared bands is applied to MODIS SWIRS bands. For Terra, noticeable drifts up to 2% depending on scan angle were previously observed in the C6.1 version of these trends. Consequently, an on-orbit RVS is applied to correct the drifts for Terra SWIR bands in C7, resulting in the more stable trends seen for C7 in Figure 11. For these bands, due to reduced reliability in SD and lunar measurements, the on-orbit RVS is characterized using DCC data. In the case of Aqua SWIR bands, both the C6.1 and C7 products continue to use the prelaunch RVS. For band 5, results show that the agreement between Terra and Aqua in C7 is within 2% across the entire scan range. Larger fluctuations in the DCC mean and mode are observed in Aqua SWIR bands than the same bands for Terra. This is likely due to a lack of BRDF correction, particularly for the SWIR bands, since the BRDF correction based on Hu's model worked reasonably well only for the VIS and NIR bands [37,41].

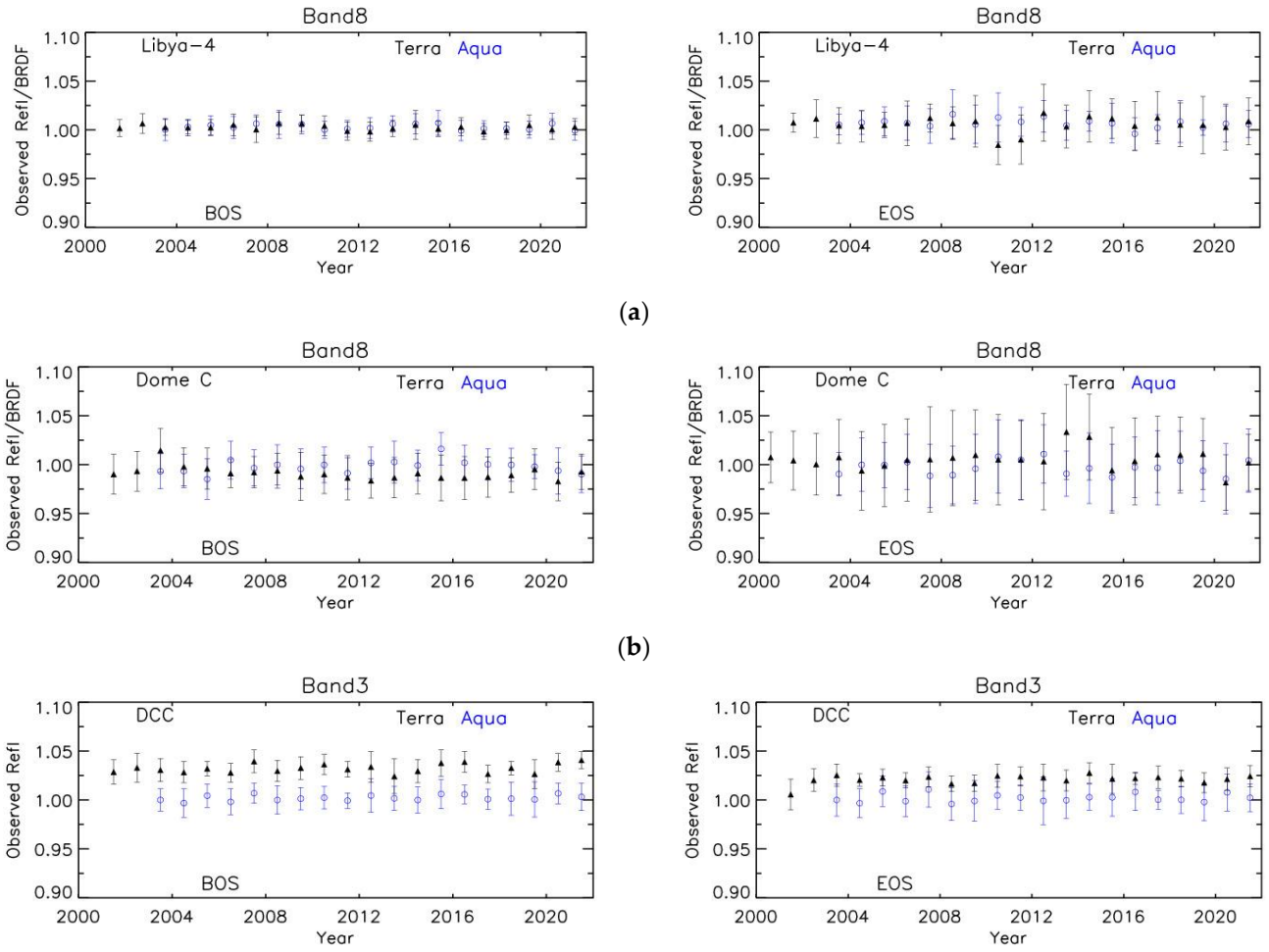



**Figure 10.** Normalized reflectance trends for Terra (solid triangle) and Aqua (open ciecle) MODIS band 8 for Libya-4 (**a**) and Dome C (**b**) and band 3 for DCC (**c**). The left side of the panel is from BOS, and the right side is from EOS.

Table 2A lists the Terra and Aqua comparison results at BOS, NAD, and EOS for all available bands, as seen in C7, determined from the various approaches. These results are obtained by averaging using trending data from 2002 to 2022 for all approaches except for SNO. The SNO approach has a relatively short data period from 2012 to the present compared with other approaches. For the VIS and NIR bands, the relative differences are within 2% for all AOIs from the four approaches. An exceptionally large difference (−3.84%) is from band 4 at EOS over the desert site, which is still unclear, and as discussed previously, it is likely related to inconsistent azimuth angles between Terra and Aqua. Further examination of the biases indicates the differences at NAD among the approaches are more consistent than those at BOS and EOS. The uncertainties from the Dome C approach are higher than other approaches. Examination of the fitting residuals of the Dome C BRDF indicates this is due to inadequacy of the BRDF correction, particularly for the NIR bands. Testing with an empirical parameterization such as those provided by Warren et al. [42] based on near-surface tower measurements at the Dome C site does not show a significant improvement over the current model. One BRDF model that depends on information on the size and shape of snow grains showed good agreement with measurements and can be useful for further study [43]. Large uncertainties are also observed at EOS for bands 8 and 9. As discussed previously, this is mainly due to a significant increase in on-orbit polarization sensitivity for Terra. Comparison results for most ocean color bands (bands 8–12) are provided in the SNO approach, which is obtained from unsaturated pixels over

the ocean. For comparison in SWIR bands, results from the DCC and desert approach are more reliable, as their uncertainties are much lower than the other two approaches. One possible reason for the large uncertainties for the SWIR bands in the SNO and Dome C approaches is their high sensitivity to clouds. For SWIR bands 7 and 26, the DCC results show more than 2% differences between Terra and Aqua. One possible reason for the relatively larger differences in the DCC SWIR bands is that the reflectance exhibits a greater dependence upon wavelength, increased sensitivity to viewing and solar illumination geometry, and the brightness temperature threshold [41]. Since a brightness temperature threshold (set at a temperature of 205 K) is used to identify DCC pixels, errors in temperature due to calibration are magnified at extremely cold scenes, which could affect the derived DCC mode reflectances for the SWIR bands. In addition, Terra SWIR bands show greater electronic crosstalk impact than Aqua due to contamination from a few thermal emissive bands. In comparison with the results from C6.1, as shown in Table 2B, there is a major improvement in the Terra and Aqua consistency at EOS for bands 8 and 9 due to applying the polarization correction for the corresponding Terra bands before their use in the RVS characterization. The correction reduces the differences from up to 6% to within 2%. There are some noticeable improvements in bands 5 and 26 due to the replacement of the prelaunch-based RVS with an on-orbit RVS for Terra.

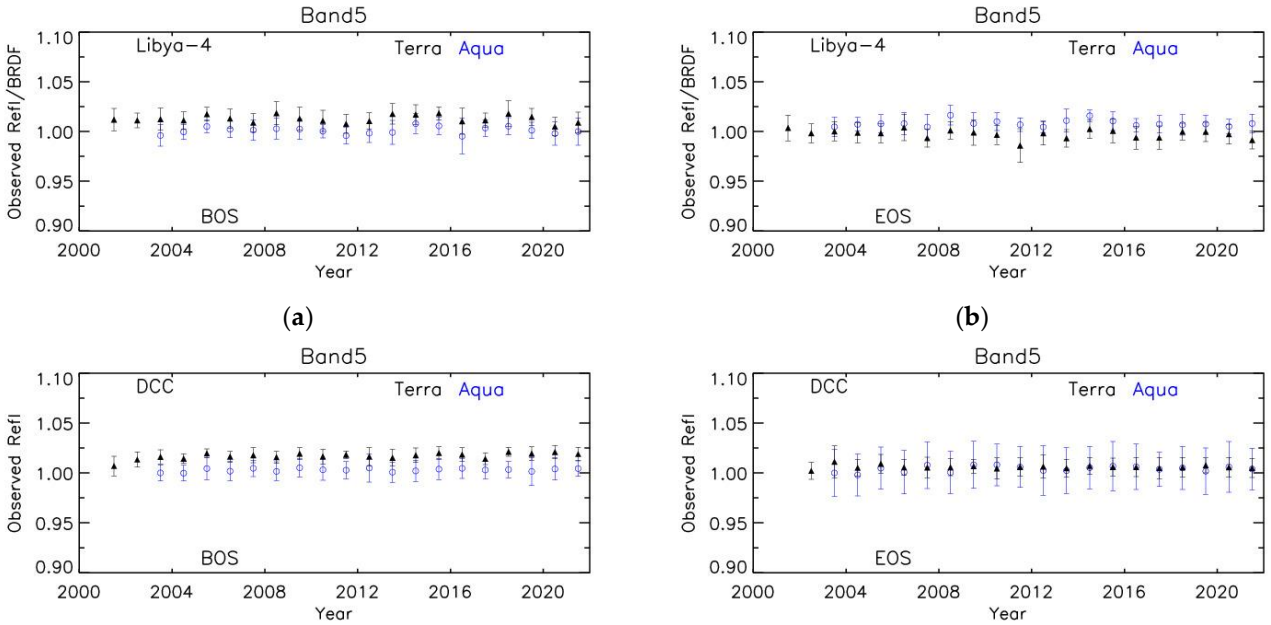



**Figure 11.** Normalized reflectance trends for Terra (solid triangle) and Aqua (open circle) MODIS band 5 for Libya-4 (**a**,**b**) and DCC (**c**,**d**). The left side of the panel is from BOS, and the right side is from EOS.

## 5. Discussion

The observed Terra and Aqua differences at BOS and NAD for the VIS and NIR bands are generally consistent to within 2% in C7. Further examination of the differences shows that Terra is slightly higher than Aqua. In comparison with C6.1, although there is a similar agreement between Terra and Aqua, C7 is more consistent across different bands due to an improved m1 fitting algorithm, particularly in the early Terra mission. As discussed in the previous section, the differences are consistent over the entire mission, indicating a possible calibration offset in prelaunch gain and RVS characterization. Since both SD gain and RVS are referenced to the prelaunch results, errors in the prelaunch characterization would be carried forward in the on-orbit measurements. The small but inconsistent differences at EOS are mainly attributed to errors in each of the four approaches. For example, the differences

for the VIS and NIR bands obtained from the Libya-4 site at EOS are negative, ranging from −0.10 to −3.8%, while results from the Dome C and DCC approaches are mostly positive, up to 2.4%. For the SWIR bands, the results are slightly worse than the VIS and NIR bands in terms of the consistency of the results among different bands and approaches, including associated larger uncertainties. Several factors contribute to a slightly worse comparison for the SWIR bands, including relatively larger uncertainties due to their high sensitivity to cloud and atmospheric conditions among these approaches and larger electronic crosstalk impact on Terra SWIR bands.

The impact of the increased polarization sensitivity for the Terra shortest wavelength bands 8, 9, and 3 mainly affects results at EOS. While adding the OBPG polarization correction in the C7 calibration algorithm has led to a significant reduction in the temporal fluctuation and gain estimation in the supplemental response data from the desert sites used to derive the gain and RVS, C7 L1B data are not corrected for polarization impact.

The MODIS spectral characterization is performed using one of its onboard calibrators, the Spectroradiometric Calibration Assembly (SRCA), designed to monitor the on-orbit spectral performance of the RSB. For both Terra and Aqua MODIS, the center wavelength and bandwidth shift over the mission are well within 1.0 nm for most RSBs. A sensitivity study of the impact of in-band RSR changes observed from SRCA and those due to degradation of the MODIS scan mirror indicates they are generally less than 0.5% in all cases at any time in the missions [44].

## 6. Conclusions

This study provides an assessment of the calibration stability of Terra and Aqua MODIS RSB and their radiometric consistency using what is to be produced by the Collection 7 reprocessed L1B. Four independent vicarious approaches based on the Libya-4 desert, Dome C, DCC, and SNO, are used to characterize the stability and radiometric assessment at the beginning, nadir, and end of the scan. Results indicate that both Terra and Aqua RSB are stable to within 1% over their mission periods using the reflectances generated internally by the C7 LUT. Comparison of the normalized reflectances by either BRDF or a common reference sensor provides a fundamental assessment of the relative consistency of radiometric calibration. Results indicate Terra VIS/NIR bands are 1–2% higher than Aqua RSB around the nadir and at the beginning of the scan for all the approaches. In the cases at the end of the scan, the agreement among the approaches is within ±2%, indicating an excellent on-orbit RVS characterization. For comparison of the MODIS SWIR bands, the differences are generally within 2%, with bands 7 and 26 up to 3%. The results of this study produce useful information about potential impacts on the comparison of future downstream science products. It also provides findings that are useful for diagnosing and improving calibration algorithms implemented in C7.

**Author Contributions:** Methodology, A.W.; Formal analysis, A.W.; Investigation, A.W.; Resources, A.A.; Data curation, A.A., Q.M. and S.L.; Writing—original draft, A.W.; Writing—review & editing, X.X., A.A., Q.M. and S.L.; Supervision, X.X. All authors have read and agreed to the published version of the manuscript.

**Funding:** This research received no external funding.

**Data Availability Statement:** Original data sets of raw digital response are provided by LAADS DAAC—NASA (https://ladsweb.modaps.eosdis.nasa.gov/, accessed on 15 October 2022). The data of C7 and C6.1 reflectances used in this study are converfted using the data of raw digital response and LUT generated by MCST. The C7 LUT is currently under science tests and has been officitally released.

**Acknowledgments:** We would like to thank Kevin Twedt and Kevin Vermeesch from the MODIS Characterization Support Team for their helpful editing and valuable comments and suggestions.

**Conflicts of Interest:** The authors declare no conflict of interest.

## References


1. Justice, C.O.; Townshend, J.R.G.; Vermote, E.F.; Masuoka, E.; Wolfe, R.E.; Saleous, N.; Roy, D.P.; Morisette, J.T. An overview of MODIS Land data processing and product status. *Remote Sens. Environ.* **2002**, *83*, 3–15. [CrossRef]
2. Esaias, W.E.; Abbott, M.R.; Barton, I.; Brown, O.B.; Campbell, J.W.; Carder, K.L.; Clark, D.K.; Evans, R.H.; Hoge, F.E.; Gordon, H.R.; et al. An overview of MODIS capabilities for ocean science observations. *IEEE Trans. Geosci. Remote Sens.* **1998**, *36*, 1250–1265. [CrossRef]
3. Parkinson, C. Aqua: An earth-observing satellite mission to examine water and other climate variables. *IEEE Trans. Geosci. Remote Sens.* **2003**, *41*, 173–183. [CrossRef]
4. King, M.; Platnick, S.; Menzel, W.P.; Ackerman, S.A.; Hubanks, P.A. Spatial and Temporal Distribution of Clouds Observed by MODIS Onboard the Terra and Aqua Satellites. *IEEE Trans. Geosci. Remote Sens.* **2013**, *51*, 3826–3852. [CrossRef]
5. Xiong, X.; Angal, A.; Twedt, K.; Chen, H.; Link, D.; Geng, X.; Aldoretta, E.; Mu, Q. MODIS Reflective Solar Bands On-Orbit Calibration and Performance. *IEEE Trans. Geosci. Remote Sens.* **2019**, *57*, 6355–6371. [CrossRef]
6. Xiong, X.; Sun, J.; Esposito, J.A.; Guenther, B.; Barnes, W.L. MODIS reflective solar bands calibration algorithm and on-orbit performance. In *Proceedings Volume 4891, Optical Remote Sensing of the Atmosphere and Clouds III*; SPIE: Bellingham, WA, USA, 2003. [CrossRef]
7. Biggar, S.F.; Thome, K.J.; Wisniewski, W. Vicarious radiometric calibration of EO-1 sensors by reference to high-reflectance ground targets. *IEEE Trans. Geosci. Remote Sens.* **2003**, *41*, 1174–1179. [CrossRef]
8. Thome, K.; Biggar, S.; Choi, H. Vicarious calibration of Terra ASTER, MISR, and MODIS. *Proc. SPIE Earth Obs. Syst. IX* **2004**, *5542*, 290–299.
9. Cao, C.; Weinreb, M.; Xu, H. Predicting simultaneous nadir overpasses among polar-orbiting meteorological satellites for intersatellite calibration of radiometers. *J. Atmos. Ocean. Technol.* **2004**, *21*, 537–542. [CrossRef]
10. Wu, A.; Xiong, X.; Cao, C. Terra and Aqua MODIS inter-comparison of three reflective solar bands using AVHRR onboard the NOAAKLM satellites. *Int. J. Remote Sens.* **2008**, *29*, 1997–2010. [CrossRef]
11. Doelling, D.R.; Haney, C.O.; Scarino, B.R.; Gopalan, A.; Bhatt, R. Improvements to the geostationary visible imager ray-matching calibration algorithm for CERES. *J. Atmos. Ocean. Technol.* **2016**, *33*, 2679–2698. [CrossRef]
12. Angal, A.; Bruegge, C.; Xiong, X.; Wu, A. Intercalibration of the reflective solar bands of MODIS and MISR instruments on the Terra platform. *J. Appl. Remote Sens.* **2022**, *16*, 027501. [CrossRef]
13. Wu, A.; Xiong, X.; Bhatt, R.; Haney, C.; Doelling, D.R.; Angal, A.; Mu, Q. An Assessment of SNPP and NOAA20 VIIRS RSB Calibration Performance in NASA SIPS Reprocessed Collection-2 L1B Data Products. *Remote Sens.* **2022**, *14*, 4134. [CrossRef]
14. Doelling, D.R.; Wu, A.; Xiong, X.; Scarino, B.R.; Bhatt, R.; Haney, C.O.; Morstad, D.; Gopalan, A. The Radiometric Stability and Scaling of Collection 6 Terra- and Aqua-MODIS VIS, NIR, and SWIR Spectral Bands. *IEEE Trans. Geosci. Remote Sens.* **2015**, *53*, 4520–4535. [CrossRef]
15. Bhatt, R.; Doelling, D.R.; Haney, C.; Scarino, B.R.; Wu, A.; Gopalan, A. Response Versus Scan-Angle Assessment of MODIS Reflective Solar Bands in Collection 6.1 Calibration. *IEEE Trans. Geosci. Remote Sens.* **2020**, *58*, 2276–2289. [CrossRef]
16. Bouvet, M.; Thome, K.; Berthelot, B.; Bialek, A.; Czapla-Myers, J.; Fox, N.P.; Goryl, P.; Henry, P.; Ma, L.; Marcq, S.; et al. RadCalNet: A Radiometric Calibration Network for Earth Observing Imagers Operating in the Visible to Shortwave Infrared Spectral Range. *Remote Sens.* **2019**, *11*, 2401. [CrossRef]
17. Cao, C.; Uprety, S.; Blonski, S. Establishing radiometric consistency among VIIRS, MODIS, and AVHRR using SNO and SNOx methods. In Proceedings of the 2012 IEEE International Geoscience and Remote Sensing Symposium, Munich, Germany, 22–27 July 2012; pp. 6928–6931. [CrossRef]
18. Wu, A.; Xiong, X.; Doelling, D.R.; Morstad, D.; Angal, A.; Bhatt, R. Characterization of Terra and Aqua MODIS VIS, NIR, and SWIR Spectral Bands' Calibration Stability. *IEEE Trans. Geosci. Remote Sens.* **2012**, *51*, 4330–4338. [CrossRef]
19. Lyapustin, A.; Wang, Y.; Xiong, X.; Meister, G.; Platnick, S.; Levy, R.; Franz, B.; Korkin, S.; Hilker, T.; Tucker, J.; et al. Scientific impact of MODIS C5 calibration degradation and C6+ improvements. *Atmos. Meas. Tech.* **2014**, *7*, 4353–4365. [CrossRef]
20. Levy, R.C.; Mattoo, S.; Sawyer, V.; Shi, Y.; Colarco, P.R.; Lyapustin, A.I.; Wang, Y.; Remer, L.A. Exploring systematic offsets between aerosol products from the two MODIS sensors. *Atmos. Meas. Tech.* **2018**, *11*, 4073–4092. [CrossRef]
21. Twedt, K.; Aldoretta, E.; Angal, A.; Chen, H.; Geng, X.; Li, Y.; Mu, Q.; Vermeesch, K.; Xiong, X. MODIS reflective solar bands calibration improvements for Collection 7. In *Proceedings Volume 11858, Sensors, Systems, and Next-Generation Satellites XXV*; SPIE: Bellingham, WA, USA, 2021. [CrossRef]
22. Angal, A.; Xiong, X.; Chang, T.; Twedt, K.; Geng, X.; Wu, A.; Aldoretta, E. Terra and Aqua MODIS collection 7 level 1B algorithm. *J. Appl. Remote Sens.* **2022**, *16*, 037502. [CrossRef]
23. Sun, J.; Xiong, X.; Angal, A.; Chen, H.; Wu, A.; Geng, X. Time-Dependent Response Versus Scan Angle for MODIS Reflective Solar Bands. *IEEE Trans. Geosci. Remote Sens.* **2014**, *52*, 3159–3174. [CrossRef]
24. Angal, A.; Xiong, X.; Wu, A.; Geng, X.; Chen, H. Improvements in the On-Orbit Response Versus Scan Angle Characterization of the Aqua MODIS Reflective Solar Bands. *IEEE Trans. Geosci. Remote Sens.* **2018**, *56*, 1728–1738. [CrossRef]
25. Kwiatkowska, E.J.; Franz, B.A.; Meister, G.; McClain, C.R.; Xiong, X. Cross calibration of ocean-color bands from moderate resolution imaging spectroradiometer on Terra platform. *Appl. Opt.* **2008**, *47*, 6796–6810. [CrossRef]
26. Wu, A.; Geng, X.; Wald, A.; Angal, A.; Xiong, X. Assessment of Terra MODIS On-Orbit Polarization Sensitivity Using Pseudoinvariant Desert Sites. *IEEE Trans. Geosci. Remote Sens.* **2017**, *55*, 4168–4176. [CrossRef]

27. Mu, Q.; Xiong, X.; Twedt, K.; Angal, A.; Geng, X. Characterization of the on-orbit response versus scan angle for Terra MODIS SWIR bands in Collection 7. *J. Appl. Remote Sens.* **2022**, *16*, 024520. [CrossRef]
28. Teillet, P.M.; Barsi, A.J.; Chander, G.; Thome, K.J. Prime candidate earth targets for the post-launch radiometric calibration of space-based optical imaging instruments. In *Proceedings Volume 6677, Earth Observing Systems XII*; SPIE: Bellingham, WA, USA, 2007; pp. 66770S-1–66770S-12.
29. Chander, G.; Xiong, X.; Choi, T.Y.; Angal, A. Monitoring on-orbit calibration stability of the Terra MODIS and Landsat 7 ETM+ sensors using pseudo-invariant test sites. *Remote Sens. Environ.* **2010**, *114*, 925–939. [CrossRef]
30. Roujean, J.-L.; Leroy, M.; Deschamps, P.Y. A bidirectional reflectance model of the Earth's surface for the correction of remote sensing data. *J. Geophys. Res.* **1992**, *97*, 20455–20468. [CrossRef]
31. Six, D.; Fily, M.; Alvain, S.; Henry, P.; Benoist, J.-P. Surface characterization of the dome concordia area (Antarctica) as a potential satellite calibration site using spot 4/vegetation instrument. *Remote Sens. Environ.* **2004**, *89*, 83–94. [CrossRef]
32. Wenny, B.N.; Xiong, X. Using a Cold Earth Surface Target to Characterize Long-Term Stability of the MODIS Thermal Emissive Bands. *IEEE Geosci. Remote Sens. Lett.* **2008**, *5*, 162–165. [CrossRef]
33. Heidinger, A.K.; Straka, W.C.; Molling, C.C.; Sullivan, J.T.; Wu, X. Deriving an inter-sensor consistent calibration for the AVHRR solar reflectance data record. *Int. J. Remote Sens.* **2010**, *31*, 6493–6517. [CrossRef]
34. Doelling, D.R.; Nguyen, L.; Minnis, P. On the use of deep convective clouds to calibrate AVHRR data. In *Proceedings Volume 5542, Earth Observing Systems IX*; SPIE: Bellingham, WA, USA, 2004. [CrossRef]
35. Doelling, D.R.; Morstad, D.; Scarino, B.R.; Bhatt, R.; Gopalan, A. The Characterization of Deep Convective Clouds as an Invariant Calibration Target and as a Visible Calibration Technique. *IEEE Trans. Geosci. Remote Sens.* **2013**, *51*, 1147–1159. [CrossRef]
36. Bhatt, R.; Doelling, D.R.; Wu, A.; Xiong, X.; Scarino, B.R.; Haney, C.O.; Gopalan, A. Initial Stability Assessment of S-NPP VIIRS Reflective Solar Band Calibration Using Invariant Desert and Deep Convective Cloud Targets. *Remote Sens.* **2014**, *6*, 2809–2826. [CrossRef]
37. Mu, Q.; Wu, A.; Xiong, X.; Doelling, D.R.; Angal, A.; Chang, T.; Bhatt, R. Optimization of a Deep Convective Cloud Technique in Evaluating the Long-Term Radiometric Stability of MODIS Reflective Solar Bands. *Remote Sens.* **2017**, *9*, 535. [CrossRef]
38. Wang, W.; Cao, C. Evaluation of NOAA-20 VIIRS Reflective Solar Bands Early On-Orbit Performance Using Daily Deep Convective Clouds Recent Improvements. *IEEE J. Sel. Top. Appl. Earth Obs. Remote Sens.* **2020**, *13*, 3975–3985. [CrossRef]
39. Hu, Y.; Wielicki, B.; Yang, P.; Stackhouse, P.; Lin, B.; Young, D. Application of deep convective cloud albedo observations to satellite-based study of terrestrial atmosphere: Monitoring stability of space-borne measurements and assessing absorption anomaly. *IEEE Trans. Geosci. Remote Sens.* **2004**, *42*, 2594–2599.
40. Xiong, X.; Angal, A.; Chang, T.; Chiang, K.; Lei, N.; Li, Y.; Sun, J.; Twedt, K.; Wu, A. MODIS and VIIRS Calibration and Characterization in Support of Producing Long-Term High-Quality Data Products. *Remote Sens.* **2020**, *12*, 3167. [CrossRef]
41. Bhatt, R.; Doelling, D.R.; Scarino, B.; Haney, C.; Gopalan, A. Development of Seasonal BRDF Models to Extend the Use of Deep Convective Clouds as Invariant Targets for Satellite SWIR-Band Calibration. *Remote Sens.* **2017**, *9*, 1061. [CrossRef]
42. Warren, S.G.; Brand, R.E.; Hinton, P.O. Effect of surface roughness on bidirectional reflectance of Antarctic snow. *J. Geophys. Res.* **1998**, *103*, 25789–25807. [CrossRef]
43. Kokhanovsky, A.A.; Zege, E.P. Scattering optics of snow. *Appl. Opt.* **2004**, *43*, 1589–1602. [CrossRef]
44. Twedt, K.A.; Angal, A.; Xiong, X. Effects of time-varying relative spectral response on the calibration of MODIS reflective solar bands. In *Proceedings Volume 10764, Earth Observing Systems XXIII*; SPIE: Bellingham, WA, USA, 2018; p. 1076413. [CrossRef]


**Disclaimer/Publisher's Note:** The statements, opinions and data contained in all publications are solely those of the individual author(s) and contributor(s) and not of MDPI and/or the editor(s). MDPI and/or the editor(s) disclaim responsibility for any injury to people or property resulting from any ideas, methods, instructions or products referred to in the content.